# Import to the inner nuclear membrane

Hapsari, Rizqiya Astri

# Chapter 2

## Long Unfolded Linkers Facilitate Membrane Protein Import Through the Nuclear Pore Complex

Anne C. Meinema,[1*] Justyna K. Laba,[1*] Rizqiya A. Hapsari,[1*] Renee Otten,[1] Frans A. A. Mulder,[1] Annemarie Kralt,[2] Geert van den Bogaart,[1†] C. Patrick Lusk,[3] Bert Poolman,[1] Liesbeth M. Veenhoff [1,2‡]

[1]Departments of Biochemistry and Biophysical Chemistry, Groningen Biomolecular Sciences and Biotechnology Institute, Netherlands Proteomics Centre, Zernike Institute for Advanced Materials, University of Groningen, Nijenborgh 4, 9747 AG, Groningen, Netherlands.

[2]Department of Neuroscience, European Research Institute on the Biology of Ageing, University Medical Centre Groningen, Groningen, Netherlands.

[3]Department of Cell Biology, Yale School of Medicine, New Haven, CT 06519, USA.

*ACM, JKL, and RAH contributed equally to this work.

‡ Corresponding author, l.m.veenhoff@rug.nl

Experiments presented in Figures 2.2 A, S3C, S4 B,C,D, S5 A were performed by RAH. This chapter was also part of the theses of Meinema & Laba and has been published in:

Meinema AC, Laba JK, Hapsari RA, Otten R, Mulder FA, Kralt A, van den Bogaart G, Lusk CP, Poolman B, Veenhoff LM. Long unfolded linkers facilitate membrane protein import through the nuclear pore complex. *Science*. 2011 Jul 1; **333**(6038): 90-3.

## Abstract

Active nuclear import of soluble cargo involves transport factors that shuttle cargo through the nuclear pore complex (NPC) by binding to phenylalanine-glycine (FG) domains. How nuclear membrane proteins cross through the NPC to reach the inner membrane is presently unclear. We found that at least a 120-residue-long intrinsically disordered linker was required for the import of membrane proteins carrying a nuclear localization signal for the transport factor karyopherin-α. We propose an import mechanism for membrane proteins in which an unfolded linker slices through the NPC scaffold to enable binding between the transport factor and the FG domains in the center of the NPC.

## Introduction

The nuclear envelope (NE) consists of an inner (INM) and outer nuclear membrane (ONM) connected by the pore membrane at sites where the nuclear pore complexes (NPCs) are embedded. The ONM is continuous with the endoplasmic reticulum (ER). NPCs are composed of a membrane-anchored scaffold that stabilizes a cylindrical central channel, in which nucleoporins (Nups) with disordered phenylalanine-glycine (FG)–rich regions provide the selectivity barrier (1). For a membrane protein to move through the NPC, its transmembrane (TM) domains must pass through the pore membrane, while its extra-luminal soluble domain(s) must pass through the NPC by a mechanism yet to be clarified (2–4). Some proteins reach the INM by diffusing through the pore membrane and adjacent lateral channels (5–8) and accumulate by binding nuclear structures (9, 10). Other membrane proteins have a nuclear localization signal (NLS), and binding to transport factors karyopherin-α and karyopherin-β1 is required to pass the NPC and reach the INM (11, 12). We sought to investigate the mechanism and path of nuclear transport of these integral INM proteins.

## Results

We first generated reporters using the *Saccharomyces cerevisiae* homolog of the human LEM domain–containing integral INM protein, Heh2. Heh2 is composed of a LEM domain, a bipartite NLS (hereafter h2NLS), a linker region (L), two TM segments flanking a luminal domain (LD), and a domain with homology to the C terminus of

MAN1 (Fig. 1A) (12). The h2NLS is recognized by Kap60 (also known as Srp1 or Karyopherin-α), the yeast homolog of human Importin-α (12). Similar to Heh2, the reporter protein h2NLS-L-TM, consisting of green fluorescent protein (GFP) fused to amino acids 93 to 378 of Heh2, accumulated specifically at the NE (Fig. 1B). A control lacking the h2NLS, named L-TM, distributed over the NE and cortical ER. Although we could not resolve the INM from the ONM, we used the average pixel intensities at the NE and ER (NE-ER ratio) as a measure of INM accumulation (fig. S2, A and B). We validated this approach by confirming the localization of h2NLS-L-TM to the INM using immuno-electron microscopy (Fig. 1C and fig. S2C). h2NLS-L-TM accumulated 33-fold at the NE (Fig. 1B), whereas L-TM accumulated only 2-fold.

Transport of h2NLS-L-TM was dependent on the Ran gradient and Nup170, similar to full- length Heh2 (Fig. 1D) (12). To confirm that the import of our membrane reporter was Kap60/95- mediated, we examined the distribution of h2NLS- L-TM in a Kap95 (Karyopherin-β–Importin-β–Rsl1) "anchor away" strain (KAP95-AA) (13). Upon addition of rapamycin, Kap95-FRB was trapped at Pma1-FKBP in the plasma membrane and no longer available for nuclear transport (fig. S2, D to F). Indeed, the accumulation of h2NLS-L-TM at the NE was markedly reduced (+RAP, Fig. 1D). Moreover, INM-localized reporter proteins redistributed to the ONM and ER upon addition of rapamycin, and the nuclear accumulation dropped with a halftime of 14 ± 2.7 min (Fig. 1E). By contrast, the fluorescence intensity of Heh2 at the NE remained unaltered for >90 min. Thus, while Heh2 is bound to nuclear factors, h2NLS-L-TM is fully mobile within the NE-ER network.

The h2NLS is a high-affinity NLS compared to the classical NLS (fig. S3). To assess whether this high affinity is required for import of h2NLS-L-TM, we replaced the bipartite h2NLS with lower-affinity NLSs: either a single-partite version of the h2NLS that lacked the first KRKR basic region (sp h2NLS) or a tandem classical NLS (tcNLS). Both membrane reporters still accumulated at the INM, but the NE/ER ratios were lower (8.1 and 4.0, respectively) than for h2NLS- L-TM (Fig. 1F), indicating a correlation between the affinity of Kap60 for an NLS and the nuclear accumulation of membrane proteins.

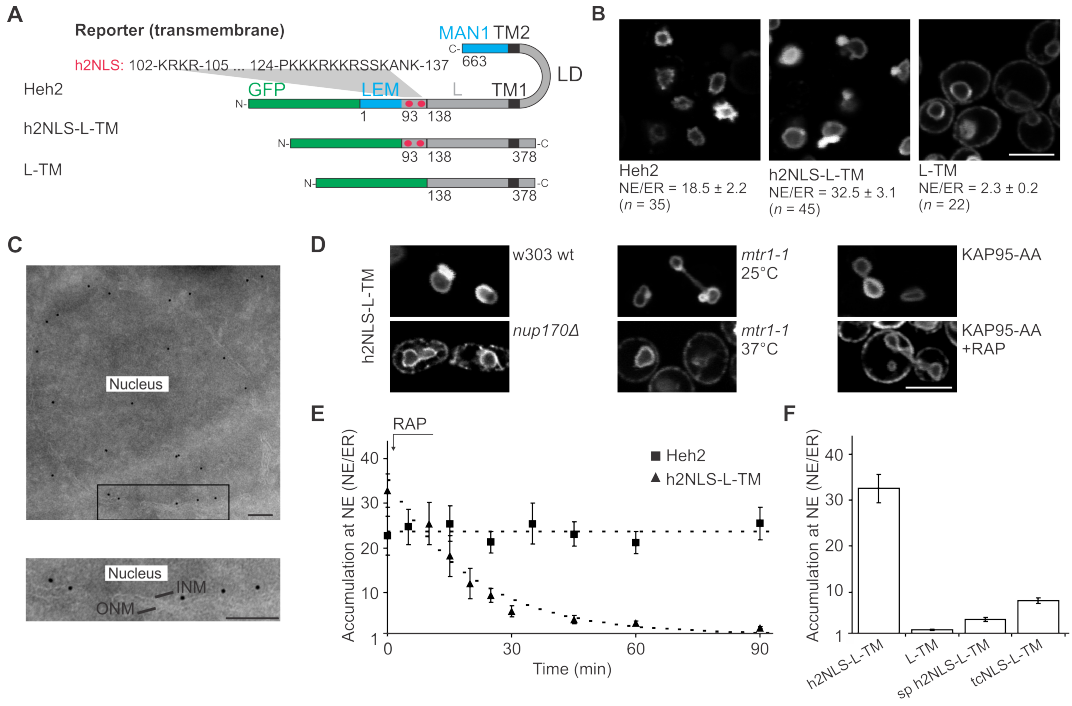


Figure 2. 1 The NLS-containing domain (h2NLS-L) of Heh2 is sufficient for accumulation at the INM. (A) Representation of Heh2-based GFP-fusion reporter proteins. (B) Confocal fluorescence images of yeast expressing the indicated proteins. Average NE/ER ratios are shown. (C) Immuno–electron micrograph of h2NLS-L-TM in the KAP95-AA strain labeled with antibodies against GFP and 10-nm-diameter gold-conjugated secondary antibody: 64% at the INM ($n$ = 350, fig. S1D). (D) h2NLS-L-TM is mislocalized in a *Nup170*Δ strain (left), in a RanGEF mutant strain (*mtr1-1*) at non-permissive temperature (middle), and in the KAP95-AA strain upon addition of rapamycin (RAP) (right). (E) The accumulation at the NE of h2NLS-L-TM (▲) and Heh2 (■) in the KAP95-AA strain as a function of time after anchoring of Kap95 (RAP at $t$ = 0, $n \geq 13$). (F) The accumulation at the INM of reporter containing a bipartite h2NLS (h2NLS-L-TM), without NLS (L-TM), with single partite NLS (sp h2NLS-L-TM), or with tandem cNLS (tcNLS-L-TM) ($n \geq 32$). SEM is indicated; scale bars: (B and D) 5 µm and (C) 250 nm

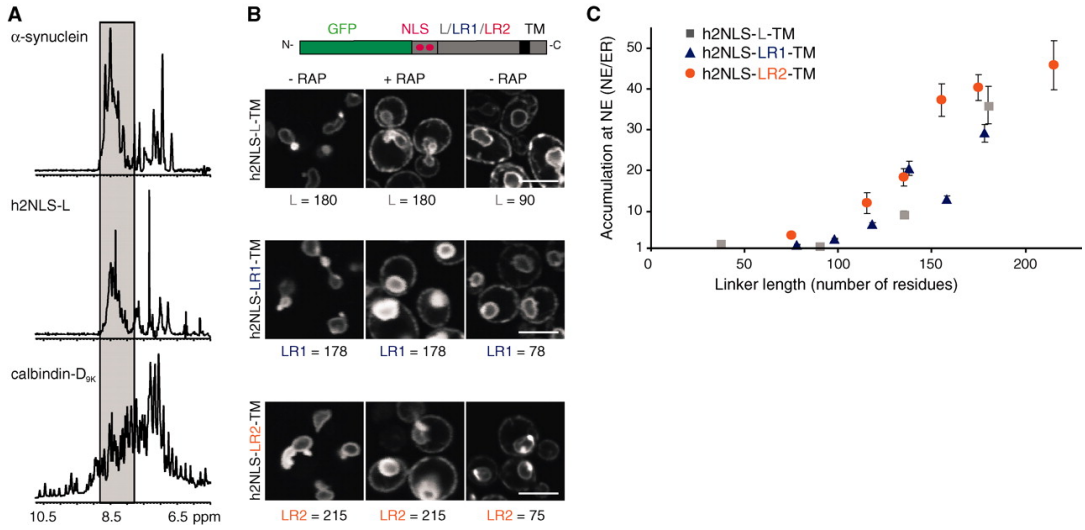


Figure 2. 2 Reporter proteins containing synthetic unfolded linkers localize at the INM. (A) One-dimensional $^1$H-NMR of the backbone amides for (unlabeled) h2NLS-L. Comparison with the intrinsically disordered α-synuclein and the folded calbindin-$D_{9k}$ show that h2NLS-L is natively unstructured. (B) Localization of the indicated reporters with native linker (L) and the randomized versions LR1 and LR2 in the KAP95-AA strain with or without rapamycin (RAP). Right panels show localization of shortened linkers. Linker length is in number of amino acids. (C) The accumulation at the NE of h2NLS-L-TM (■), h2NLS-LR1-TM (▲) and h2NLS-LR2-TM (●) and truncations thereof, plotted against the length of the linker domain ($n \geq 20$). SEM is indicated; scale bars: 5 µm.

We then examined how the L domain contributes to targeting. The amino acid composition of the L domain and the large Stokes radius (45 Å) of purified recombinant h2NLS-L suggest that it is unstructured (fig. S4, A to C). In addition, nuclear magnetic resonance (NMR) spectra of (unlabeled) h2NLS-L were typical of disordered proteins. The absence of stable secondary and tertiary structure was gauged from a lack of signal dispersion of the backbone amides for h2NLS-L in one-dimensional 1H-NMR spectra (Fig. 2A, shaded area) and of the side-chain methyl signals in [1H-13C]-HSQC (heteronuclear single-quantum coherence) spectra (fig. S4D). To evaluate whether the sequence of the linker region contributed to targeting, we replaced the coding regions of the L domain in h2NLS-L-TM with two synthetic sequences, LR1 and LR2. These were generated randomly but had the same relative amino acid abundance as L. LR1 and LR2 are also predicted to be unfolded (fig. S4A). Both h2NLS-LR1-TM and h2NLS-LR2-TM were efficiently transported to the INM in a Kap-dependent manner (Fig. 2B). Systematic truncations of LR1 and LR2 and the original linker (L) resulted in three sets of reporters with variable linker lengths (see tables S2 and S3). The shortest truncations of each linker set did not accumulate at the nucleus (Fig. 2B). Indeed, we observed a marked dependence of INM import on linker length (Fig. 2C). Reporters with a synthetic TM segment and reporters with 1, or all 10 TM segments of an ER protein, Sec61, were also efficiently imported to the INM (Fig. 3). An "NLS-L-TM"-sorting signal could be recognized in Heh1 and, indeed, its NLS-linker-domain, even though lacking homology to that of Heh2, promoted INM targeting (fig. S5A).

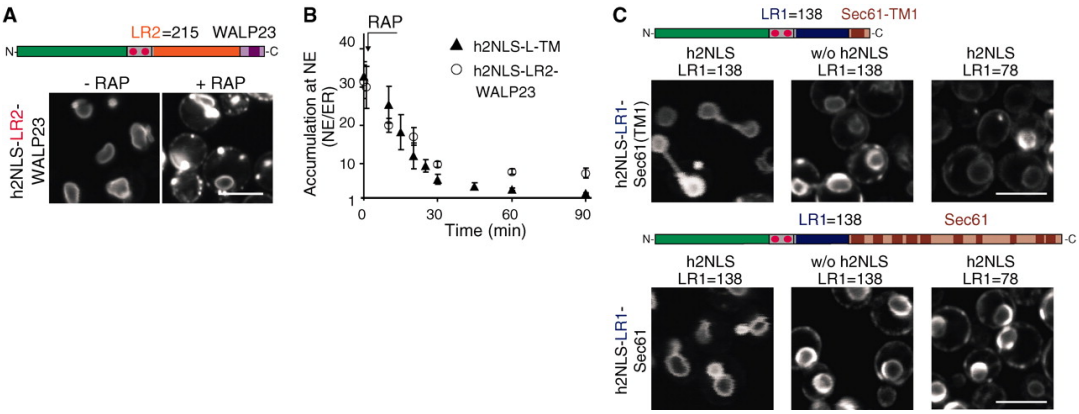


Figure 2. 3 Synthetic TM peptides and ER proteins can be targeted to the INM. (A) Representation of h2NLS-LR2 fused to the WALP23 TM region and images of its localization with or without rapamycin (RAP). (B) After addition of rapamycin, the reporter h2NLS-LR2-WALP23 leaked to the ER with kinetics similar to that displayed by h2NLS-L-TM. (C) NE localization of h2NLS-LR1(138) reporters containing the first TM of Sec61 (top, left) and full-length Sec61 (bottom, left). Without the h2NLS (middle) and with the shorter linker, LR1(78) (right), accumulation is lost. SEM is indicated; scale bars: 5 µm.

Next, we determined whether the transport of the reporters across the NPC depends on specific FG regions of nucleoporins (14–16). A strain that lacks the GLFG repeats of Nups 100, 145, and 57 (17), which are anchored to both the cytoplasmic and nucleoplasmic halves of the NPC scaffold (18), showed 7.5-fold decreased NE accumulation (SWY2950, Fig. 4A). Minimal effects were seen with single deletions (fig. S5B) and in strains lacking the FG regions from the asymmetric localized Nups (SWY3062, SWY3042), whereas Kap60/95-mediated transport of soluble cargo (tcNLS-GFP) was affected in all three strains.

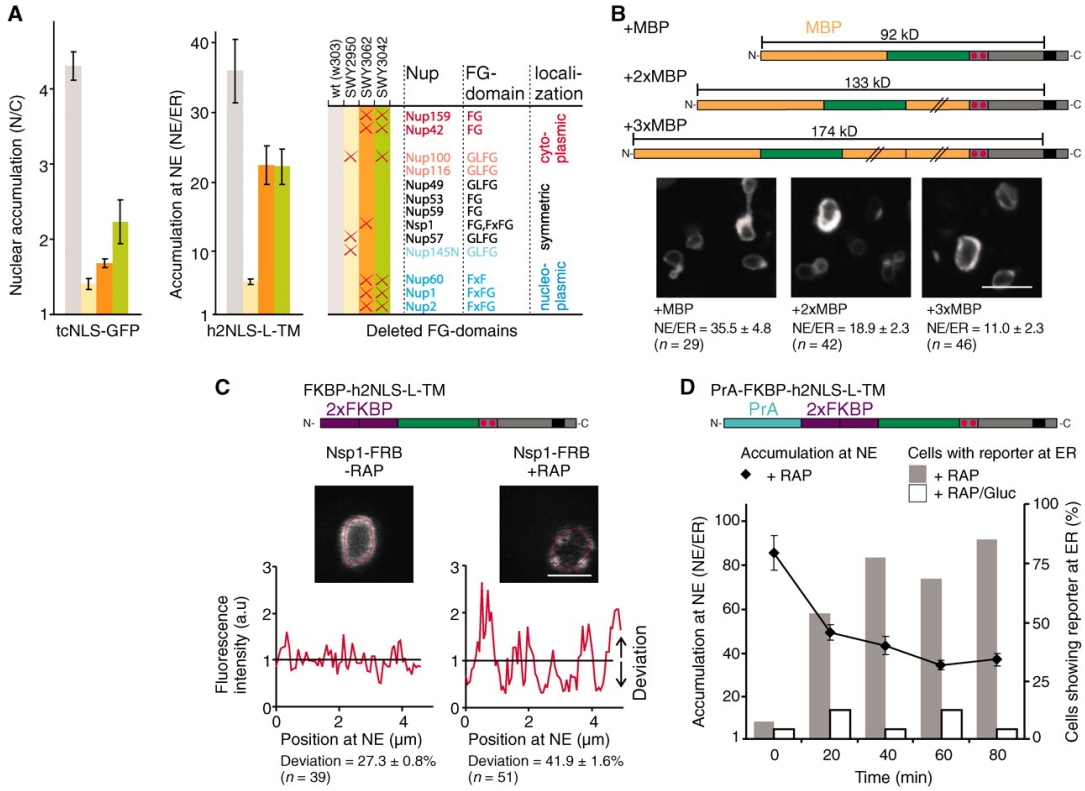


Figure 2. 4 Membrane protein reporters interact with central-channel FG-Nups during import. (A) The nuclear accumulation of tcNLS-GFP (soluble) and h2NLS-L-TM, in wild-type and mutant strains with FG-domain deletions ($n \geq 21$) (*17*). (B) Localization of reporters containing soluble domains of increasing size. The accumulation at the NE is indicated. (C) Localization of a reporter with an N-terminal FKBP tag in a strain expressing Nsp1-FRB before (left) and after addition of rapamycin (right). Trapping of FKBP-tagged reporter at NPCs is apparent from punctate staining; the deviation in fluorescence at the NE is higher in the presence of rapamycin. (D) Rapamycin-dependent trapping of PrA-FKBP–tagged reporter at Nsp1-FRB blocked import as observed from increased ER-localized reporter. Percentage of cells showing fluorescence at the ER ($n \geq 100$, bars) and the average NE/ER ratio ($n \geq 13$, symbols) upon addition of rapamycin (RAP, filled bars and ♦) or glucose (inhibition of reporter synthesis) and rapamycin (RAP/Gluc, open bars). SEM is indicated; scale bars: (B) 5 µm and (C) 2 µm.

Our data point toward passage of the extra-luminal soluble domains of the membrane proteins through the central channel, which is expected to place few constraints on the bulkiness of these domains. Indeed, membrane proteins with up to 174-kD soluble domains were imported to the INM, although the efficiency decreased with increasing size (Fig. 4B). To further support the suggestion that the extraluminal

soluble domains pass through the central channel, we designed experiments to trap the reporters in transit through the NPC. We constructed a strain expressing FRB-tagged FG-Nup Nsp1. The C-terminal FRB tag on Nsp1 is anchored on the pore side of the scaffold of the NPC (16, 18–20). A reporter containing FKBP at its N terminus was expressed to enable rapamycin-dependent trapping at Nsp1-FRB in the NPC (fig. S5C). Addition of rapamycin yielded a punctate stain typical of NPC-localized proteins; without rapamycin the reporter distributed evenly over the NE (Fig. 4C and fig. S5D). Next, we assessed whether trapping of the reporter at the NPC affected transport. We used a reporter expressed at higher levels (with an additional N-terminal protein A tag) and saw a blockage of INM import and steady increase in fluorescence at the ER from newly synthesized proteins, after rapamycin addition (Fig. 4D and fig. S5E). Trapping of the reporter specifically blocked transport of membrane proteins and not soluble proteins (fig. S5, F and G). Thus, the h2NLS-containing the N-terminus of the reporter passes where Nsp1 is anchored to the NPC scaffold and within the central channel of the NPC.

Here, we have elucidated the NLS-dependent mechanism of membrane protein transport through the NPC. The Heh2-derived reporter proteins ac- cumulate at the INM, not because they are retained or trapped at the INM, but because Kap60/95-mediated import is faster than export. The signal for targeting to the INM is composed of a natively unfolded linker that spaces the TM segment and a high-affinity NLS. It takes little energy to stretch the linker to allow the NLS, with bound karyopherins, to dodge between the NPC scaffold and the karyopherins to bind the FG-Nups (fig. S6). The proposed transport route implies that, at least transiently, openings must exist between the space immediately aligning the pore membrane and the central channel. At present, structures of the NPC lack the resolution to reveal such conduits, but its plasticity and the overall lattice-like scaffold structure observed in electron microscopy (8, 21, 22) and computational structures (18) are compatible with our model. The transport mechanism described here is likely to exist in parallel with a previously proposed route based on diffusion and nuclear retention (2, 5–7, 9, 10).

## Acknowledgments

We thank M. C. King, M. P. Rout, and D. J. Slotboom for discussion; V. Krasnikov for help with confocal microscopy; and M. Graham for assistance with immunoelectron

microscopy. We thank S. R. Wente, U. K. Laemmli, and M. P. Rout for reagents and strains. This work was supported by funding from the Netherlands Organization for Scientific Research (VIDI fellowship to L.M.V. and F.A.A.M.; Top-subsidy grant 700.56.302 to B.P.).

## Author contribution

L.M.V. conceived the project. Experiments were performed and analyzed by A.C.M., J.K.L., R.A.H. (Figures 2.2 A; S3 C; S4 B, C, D; S5 A ), C.P.L., and A.K. NMR was performed by R.O. and F.A.A.M. G.v.d.B. helped with image analysis. Experiments were designed and the manuscript was written by A.C.M., C.P.L., B.P., and L.M.V.

## References

1. S. R. Wente, M. P. Rout, Cold Spring Harb. Perspect. Biol. 2, a000562 (2010).
2. N. Zuleger, N. Korfali, E. C. Schirmer, Biochem. Soc. Trans. 36, 1373 (2008).
3. C. P. Lusk, G. Blobel, M. C. King, Nat. Rev. Mol. Cell Biol. 8, 414 (2007).
4. T. Ohba, E. C. Schirmer, T. Nishimoto, L. Gerace, J. Cell Biol. 167, 1051 (2004).
5. P. Malik *et al.*, Cell. Mol. Life Sci. 67, 1353 (2010).
6. B. Soullam, H. J. Worman, J. Cell Biol. 130, 15 (1995).
7. W. Wu, F. Lin, H. J. Worman, J. Cell Sci. 115, 1361 (2002).
8. J. E. Hinshaw, B. O. Carragher, R. A. Milligan, Cell 69, 1133 (1992).
9. J. Ellenberg *et al.*, J. Cell Biol. 138, 1193 (1997).
10. C. Ostlund, J. Ellenberg, E. Hallberg, J. Lippincott-Schwartz, H. J. Worman, J. Cell Sci. 112, 1709 (1999).
11. Y. Turgay *et al.*, EMBO J. 29, 2262 (2010).
12. M. C. King, C. P. Lusk, G. Blobel, Nature 442, 1003 (2006).
13. H. Haruki, J. Nishikawa, U. K. Laemmli, Mol. Cell 31, 925 (2008).
14. S. Frey, R. P. Richter, D. Görlich, Science 314, 815 (2006).
15. R. Peters, Bioessays 31, 466 (2009).
16. M. P. Rout *et al.*, J. Cell Biol. 148, 635 (2000).
17. L. A. Strawn, T. Shen, N. Shulga, D. S. Goldfarb, S. R. Wente, Nat. Cell Biol. 6, 197 (2004).
18. F. Alber *et al.*, Nature 450, 695 (2007).
19. N. Schrader *et al.*, Mol. Cell 29, 46 (2008).
20. S. M. Bailer, C. Balduf, E. Hurt, Mol. Cell. Biol. 21, 7944 (2001).
21. D. Frenkiel-Krispin, B. Maco, U. Aebi, O. Medalia, J. Mol. Biol. 395, 578 (2010).
22. Q. Yang, M. P. Rout, C. W. Akey, Mol. Cell 1, 223 (1998).

## Supplementary Information

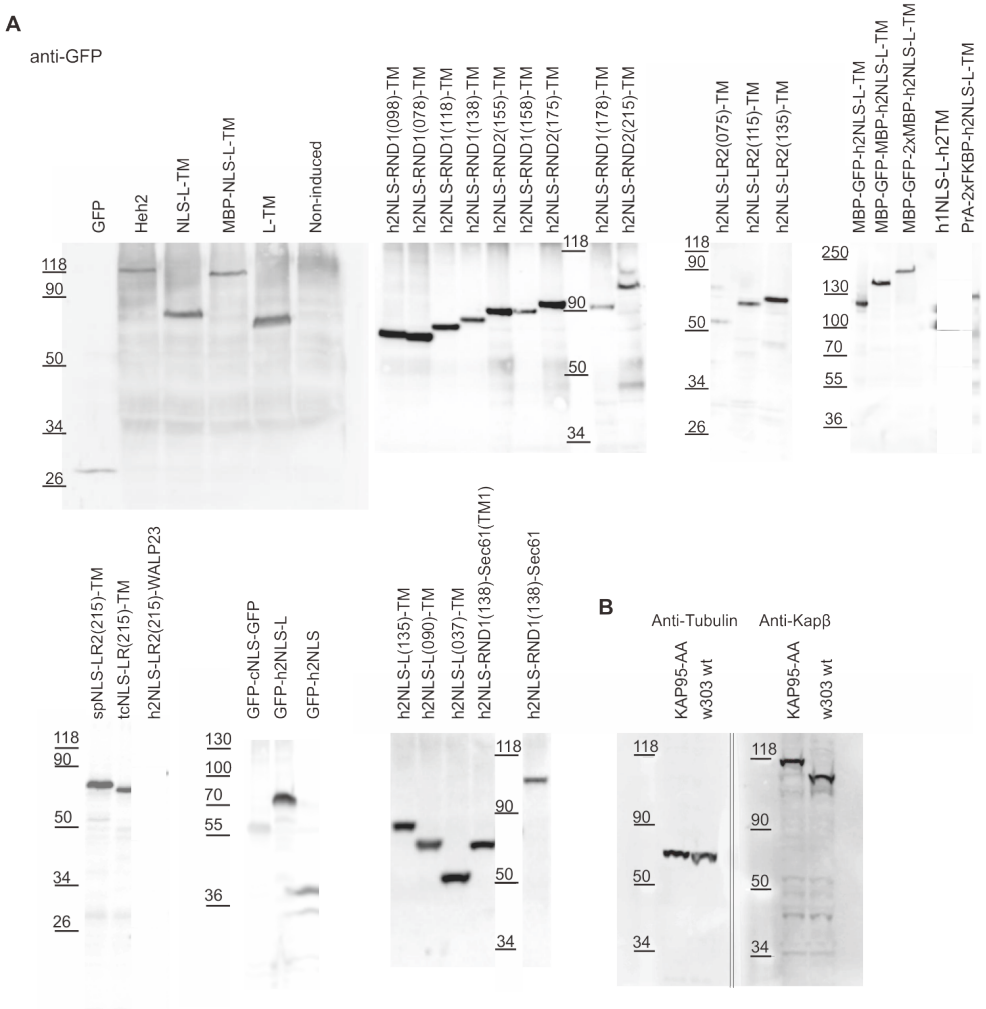


Figure S 1 Western blot of whole cell extracts showing the expression of various proteins. (A) Cells were grown to 107 cells per mL, and, after 2 hours of induction with 0.1% (w/v) D-galactose, whole cell lysates were prepared. For immuno-detection, an anti-GFP antibody was used. (B) The concentration of Kap95 was determined in wild-type and KAP95-AA strains, expressing h2NLS-L-TM. Cells were grown to 107 cells per mL, an equivalent of 7 × 106 cells was loaded onto the gel. The increase in molecular weight is due to the presence of the 14 kDa FRB-tag. The expression in S. cerevisiae w303 of Kap95-tagged with FRB is similar to that of wild-type Kap95. Tubulin levels were used as a loading control.

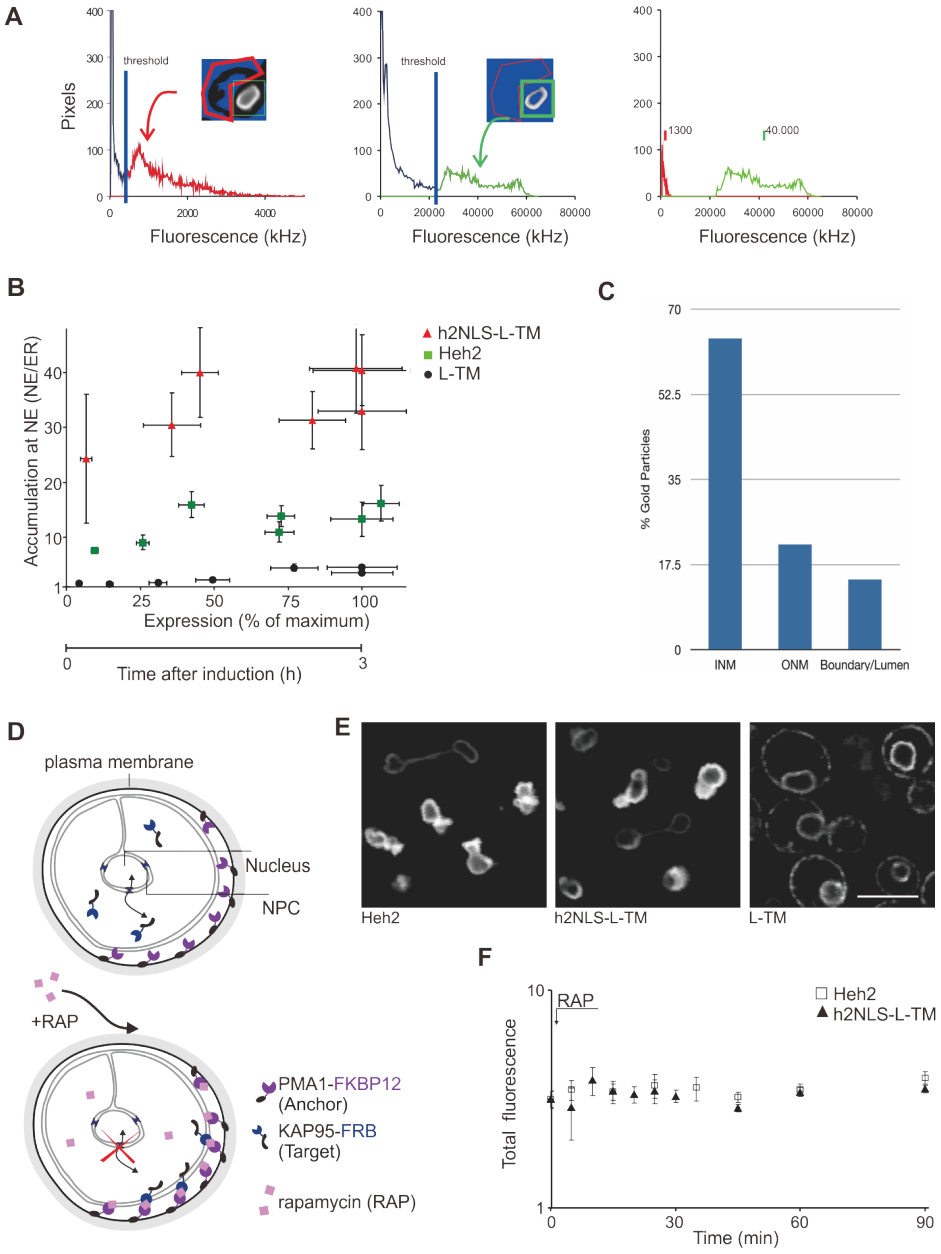


Figure S 2 Membrane reporter proteins accumulate at INM. (A) Image analysis to determine the accumulation levels. In a typical confocal image of a cell expressing h2NLS-L-TM, the area of the nucleus (red box) and the ER were selected (green box) as indicated. The corresponding distributions of the pixel fluorescence intensities in the entire selected areas are plotted in a histogram for the ER (left) and the NE (middle). The histogram shows two populations of pixels: the low fluorescence intensity pixels correspond to background and out-of-focus signal and the high intensity pixels to the focused signal at the membranes of the cell. A mask was created to exclude all the low intensity pixels. Therefore a minimum threshold was set between these populations. The values of the pixels not excluded by the mask in the image are plotted in the graphs: in red for the focused signal at the ER (left) and green for the INM (middle), and combined in one graph (right). The accumulation is defined as the mean fluorescence intensity in the NE (in this case 40,000) divided by the mean fluorescence intensity in the ER (here 1,300, thus the NE/ER-ratio was 31). The difference in NE/ER-ratio in a double blind test was <10% (n = 26). (B) Quantification of the average accumulation at the NE plotted at different expression levels of h2NLS-L-TM (red ▲), L-TM (black ●) and Heh2 (green ■), when expressed in the KAP95-AA strain. The NE-accumulation levels of the reporters are plotted against the normalized fluorescence of the cell during 3 hours. (n ≥ 18). (C) Quantification of localization of gold particles in the immuno-electron micrographs. Gold particles were localized close to the inner nuclear membrane (INM), outer nuclear membrane (ONM) or ambiguous between the membranes (Boundery/Lumen) (n = 350). (D) Schematic representation of the trapping of Kap95-FRB (Target) to Pma1-FKBP (Anchor) at the plasma membrane upon addition of rapamycin. Without rapamycin, Kap95-FRB facilitates nuclear import but after addition of rapamycin a ternary complex of FKBP12 and the FRB with nanomolar affinity (11) is formed. The cell is then depleted of functional Kap95-FRB, and

all cargo import to the nucleus that is mediated by Kap95-FRB is abolished. (E) Confocal fluorescence images of KAP95-AA strain expressing the reporter proteins Heh2, h2NLS-L-TM and L-TM tagged with GFP. The localization of these reporters was similar to that in wild-type cells (Fig. 1B): Heh2 and h2NLS-L-TM were accumulated at the NE while L-TM was localized throughout the NE-ER network. (F) Addition of rapamycin did not affect the cellular reporter levels. The average fluorescence of a cell is plotted for Heh2 (□) and h2NLS-L-TM (▲) after addition of rapamycin. The total average fluorescence of a cell is the weighted average of the intensities at the surface of the NE and the ER. To calculate the surface of the double membrane of the NE (~16 μm2) and ER (~150 μm2), the diameter of the nucleus and the ER was obtained as described previously(9) and is consistent with earlier results(20). The volumes bounded by the ER and the nuclear membranes were assumed to be spherical. The fluorescence intensities were normalized to time zero, i.e. before the addition of rapamycin. SEM is indicated, scale bar is 5 μm.

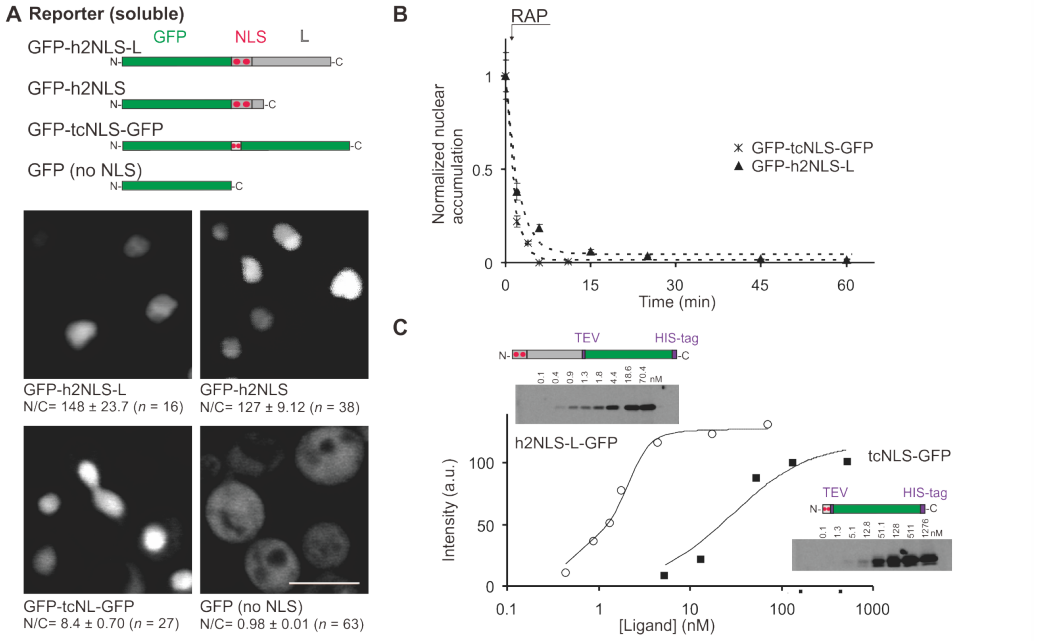


Figure S 3. The h2NLS-cargo is efficiently targeted to the nucleus because of high-affinity binding to Kap60. (A) Representation of soluble reporters (i) GFP-h2NLS-L, (ii) GFP-h2NLS (L is truncated to 27 residues) and (iii) GFP-tcNLS-GFP (tandem SV-40 classical NLS, fused to two copies of GFP) and (iv) GFP alone. The confocal fluorescence images show the localization of the reporters in live cell imaging. We quantified the concentration of reporter in the nucleus (N) and in the cytosol (C) and calculated the N/C ratio as described in fig. S2A. The cytosolic fluorescence signal in cells expressing h2NLS-L and h2NLS was close to cellular auto-fluorescence levels. We did not correct for it, so the N/C-ratio is an underestimation. (B) The accumulation of both reporters h2NLS-L fused to GFP (53 kDa) and tcNLS fused to two copies of GFP (56 kDa) was measured after adding rapamycin (RAP) in the KAP95-AA strain to evaluate the nuclear efflux. The accumulation was normalized to t = 0, i.e. before addition of rapamycin. Regardless of the high accumulation of GFP-h2NLS-L (N/C ratio of 148, panel A), the efflux could be fitted with a mono-exponential decay function with only a slightly slower efflux than GFP-tcNLS-GFP (i.e. half-times t0.5 = 89 ± 10 s) and (t0.5 = 56 ± 4 s, respectively)(n ≥ 14). High accumulation of GFP-h2NLS-L is thus not a result of trapping. (C) An in vitro solid phase binding assay with purified Kap60 lacking the Importin-β binding domain, Kap60ΔIBB, and with purified tcNLS-GFP (○) and h2NLS-L-GFP (■). Beads with Kap60ΔIBB were incubated with different concentration of cargo (ligand) and the binding (intensity) was determined from in-gel fluorescence (inset) and fitted with a simple model for binding kinetics to yield affinities (dissociation constants) of 27 nM for tcNLS-GFP (similar as in (21)) and <1 nM for h2NLS-L-GFP. SEM is indicated, scale bar is 5 μm.

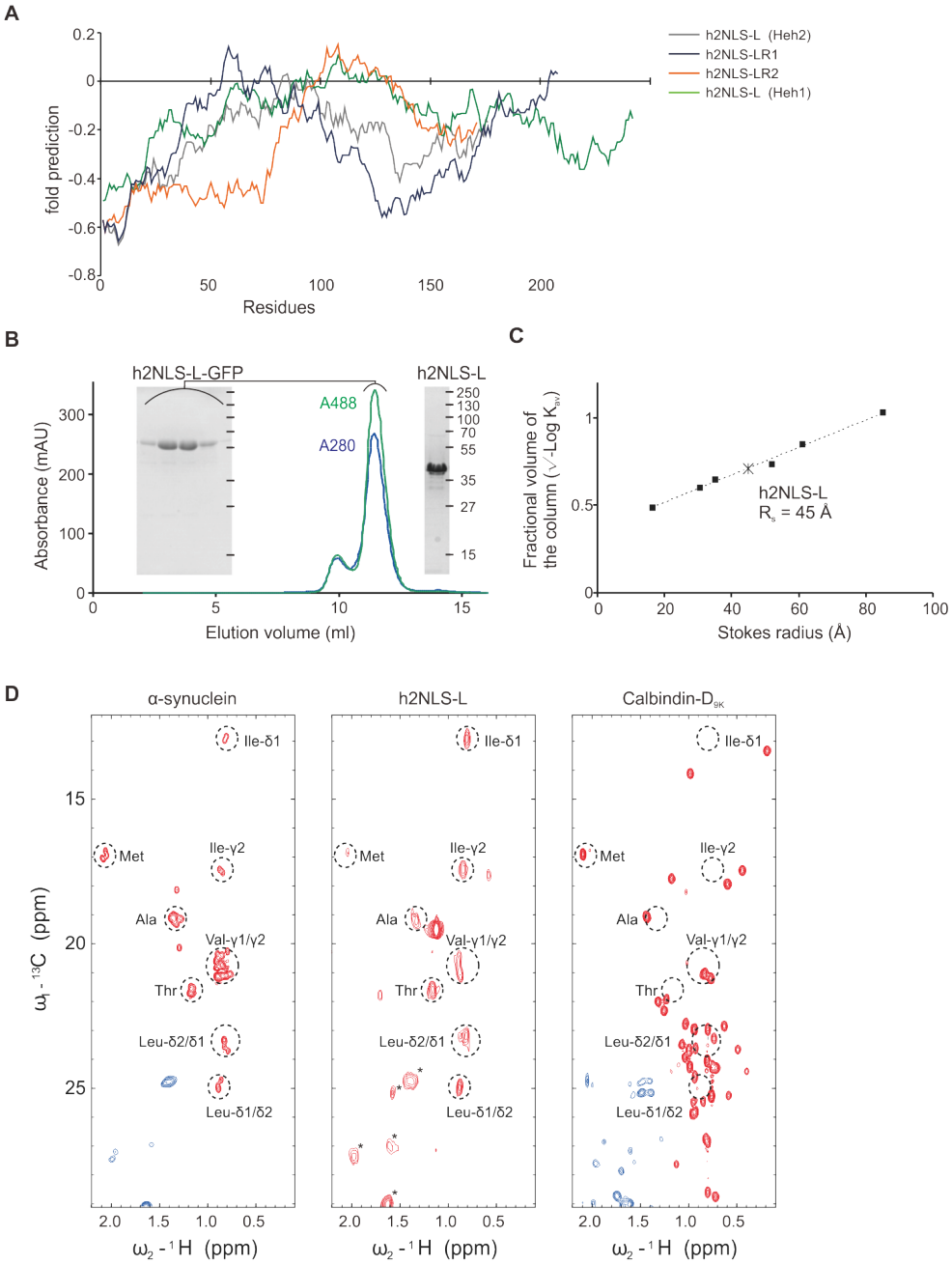


Figure S 4 The h2NLS-L protein contains a natively unfolded linker and a high-affinity NLS. (A) Prediction of FoldIndex (5) for the propensity to fold for h2NLS-L from Heh2 and h1NLS from Heh1 as well as for h2NLS-LR1 and h2NLS-LR2. A negative value indicates that the peptide is predicted to be unstructured. (B) The elution profile from size-exclusion chromatography of h2NLS-L-GFP (containing a TEV-site and a His-tag, see fig. S3B, expressed in L.lactis) and a CBB-stained SDS-PAGE gel of peak fractions (left inset). The CBB-stained SDS-PAGE gel of h2NLS-L after removal of GFP by TEV-cleavage is also shown (right). (C) The Stokes radius of the purified h2NLS-L domain (25.5 kDa) determined by SEC was 45 Å. This is in line with an expected radius for an unfolded domain or extended coil (47 ± 17 Å) and different than a radius expected for a folded or globular domain (22 ± 7 Å), according to prediction models (SD is indicated) (16, 17). The calibration with protein standards is shown. (D) Methyl region of the [1H-13C]-HSQC spectrum of the intrinsically-disordered protein human α-synuclein (left), h2NLS-L (middle), and the folded protein calbindin D9k (right)(15). The dotted circles designate the typical positions of methyl groups of the different amino acid types in disordered proteins. Signals in blue or indicated with an asterisk originate from methylene- and methine-groups in the amino acid side chains. Dispersion of spectral correlations of methyl groups outside the regions shown is indicative of a folded protein/domain. Comparison of the spectrum of h2NLS-L with a disordered (middle) and folded (right) protein unambiguously establishes the disordered nature of h2NLS-L.

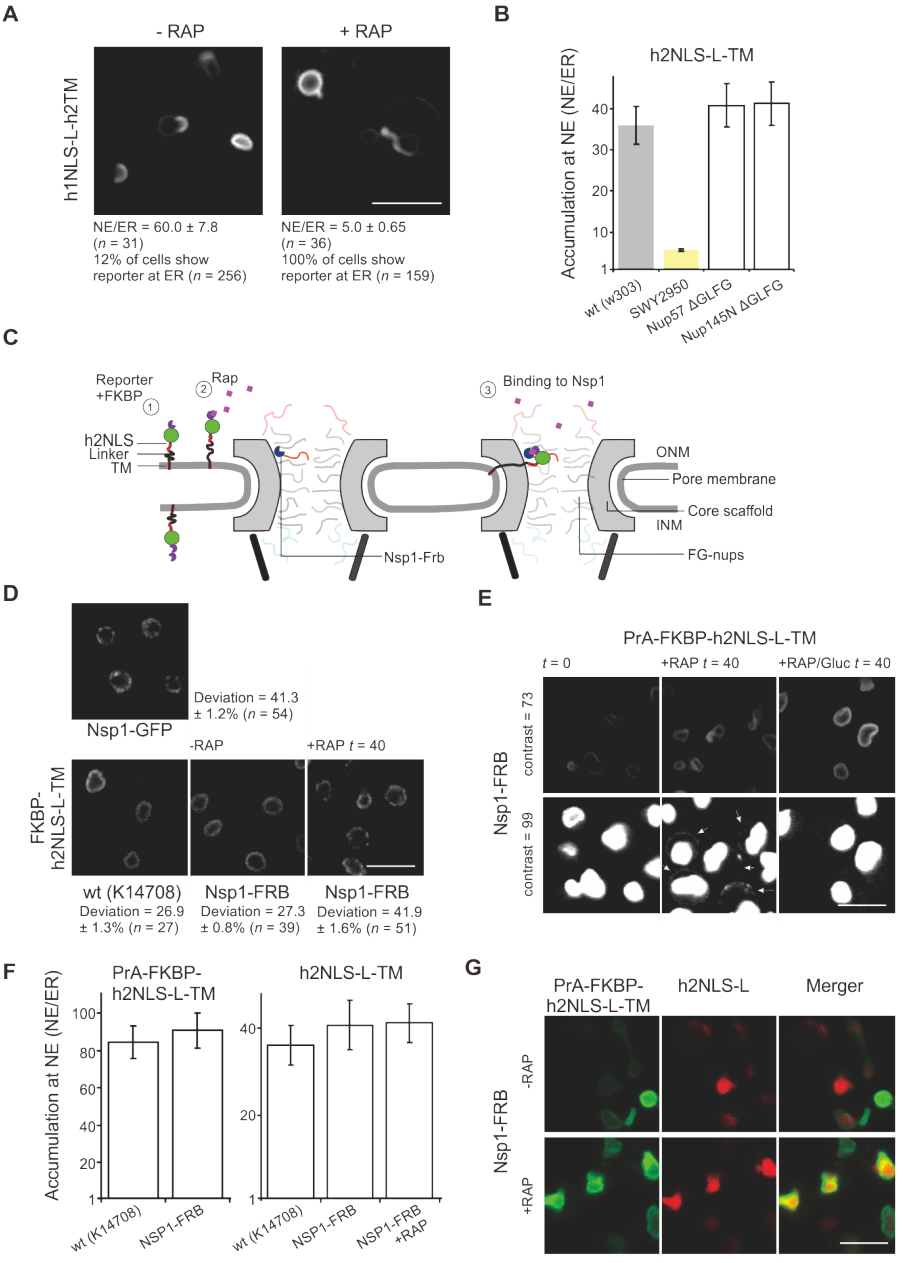


Figure S 5 Membrane protein reporters interact with central channel FG-Nups during import. (A) Heh1 is a homolog of Heh2 and has a similar "NLS-L-TM"-signature, but the h1NLS-L-TM of Heh1 is not conserved (identity score <0.18) and the linker domain in Heh1 is longer (230 residues) than Heh2 (180 residues). To test whether the h1NLS-L domain is sufficient for INM targeting, we fused it to the TM of Heh2 and measured nuclear accumulation. The confocal images show a strong accumulation (NE/ER) of 60.0-fold at the INM. After adding rapamycin (RAP) the reporter leaked out the nucleus, showing that the accumulation was Kap95-dependent. (B) The accumulation of h2NLS-L-TM at the NE is only affected when a combination of FG-domains is deleted. The accumulation in the strain SWY2950 (yellow bar), where the GLFG-domains of Nup100, Nup57 and Nup145N are deleted, is decreased compared to wild-type cells (wt, w303, grey bar). When the GLFG-domains of a single Nup57 or Nup145N were deleted, the accumulation at the NE was not affected (n ≥ 24). (C) In order to trap the N-terminus of the reporter at the pore side of the nucleus, a 2×FKBP was fused to the N-terminus of the h2NLS-L-TM reporter (1). FRB was fused to the C-terminus of Nsp1, an FG-Nup that is present in multiple copies and anchored to the NPC scaffold by its C-terminal domain. Once rapamycin is added to the medium it will bind to the FKBP at the reporter (2), enabling the FKBP to bind to FRB (3). (D) Confocal fluorescence image with the localization of Nsp1-GFP at the NPC (deviation of fluorescence at the NE is indicated) showing a punctate stain at the NE, typical for NPC-localized proteins. The localization of FKBP-h2NLS-L-TM in a strain expressing Nsp1-FRB before addition of rapamycin (RAP) show a uniform stain at the NE similar to the localization of the reporter in a wild-type (K14708) strain. Confocal image of FKBP-h2NLS-L-TM in Nsp1 after 40 minutes incubation with rapamycin (RAP) show a similar punctate stain at the

NE as for NPC-localized proteins (deviation of fluorescence at the NE is similar to Nsp1-GFP). (E) Confocal fluorescence images show localization of a reporter containing an N-terminally PrA-FKBP-tag in a strain expressing Nsp1-FRB. Before rapamycin-dependent trapping to Nsp1, the reporter accumulates at the INM (left); after addition of rapamycin (RAP) the reporter binds to Nsp1-FRB and blocks the transport pathway so newly synthesized reporter proteins no longer have access to the INM and stay at the ER (middle, arrow indicates ER-localized reporter). In controls where expression of new reporter was inhibited by addition of glucose while rapamycin was added (RAP/Gluc, right), no reporter was found at the ER, implying that INM-cumulated reporter does not leak out to the ER under these conditions. Images are shown with increased contrast settings to visualize the ER (bottom). No punctated NE is visible, because the expression of PrA-FKBP-tagged reporter is 10× higher than the FKBP-tagged reporter. (F) The nuclear accumulation of the FKBP-reporter was similar in wt (K14708) and Nsp1-FRB. Moreover, the nuclear accumulation of h2NLS-L-TM in Nsp1-FRB was similar to wt (K14708), and not affected by addition of rapamycin. The NE/ER ratio's of FKBP-h2NLS-L-TM should be considered a lower limit as they are based on the small fraction of cells (5%) that show fluorescence at the ER. See methods for details, (n ≥ 16). (G) Confocal images of NSP1-FRB cells show the expression of FKBP-h2NLS-L-TM fused to GFP (left; green), that of h2NLS-L fused to mCherry (middle; red), and the merger (right). The nuclear accumulation of the soluble h2NLS-L-mCh was similar in the absence (top) or presence (bottom) of rapamcyin. This means that the NPCs are still functional for transport of non-membrane reporter proteins bearing the same h2NLS. SEM is indicated, scale bars are 5 µm.

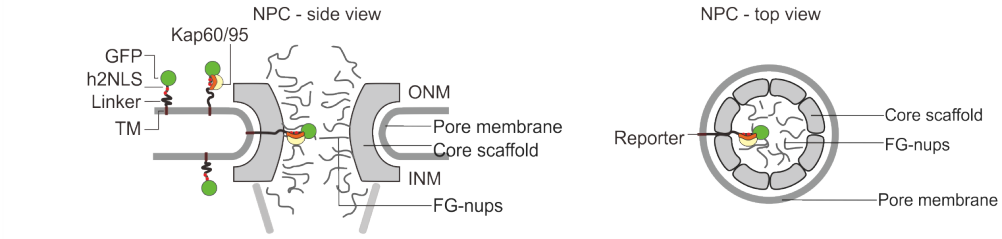


Figure S 6 Model for active nuclear import of membrane proteins. Prior to transport over the NPC, Kap60/95 binds the high affinity h2NLS of the membrane reporter. It will not take much energy to stretch the intrinsically disordered linker, to allow the Kap60/95 bound to the h2NLS, to interact with